Title

Seasonal and long-term variations in leaf area of Congolese rainforest

Authors

Sun, Yuanheng

Knyazikhin, Yuri

She, Xiaojun

et al.

Publication Date

2022

DOI

10.1016/j.rse.2021.112762

Seasonal and long-term variations in leaf area of Congolese rainforest

Yuanheng Sun[1, 2], Yuri Knyazikhin[1], Xiaojun She[1, 3], Xiangnan Ni[1, 4], Chi Chen[1, 5], Huazhong Ren[2] and Ranga B. Myneni[1]

[1]Department of Earth and Environment, Boston University, Boston, MA 02215, USA
[2]School of Earth and Space Sciences, Peking University, Beijing, China
[3]School of Geographic Sciences, Southwest University, Chongqing, China
[4]Department of Earth and Environmental Sciences, Xi'an Jiaotong University, Xi'an, China
[5]Department of Earth and Environmental Sciences, Lawrence Berkeley National Laboratory, Berkeley, CA 94720, USA

Abstract

It is important to understand temporal and spatial variations in the structure and photosynthetic capacity of tropical rainforests in a world of changing climate, increased disturbances and human appropriation. The equatorial rainforests of Central Africa are the second largest and least disturbed of the biodiversly-rich and highly productive rainforests on Earth. Currently, there is a dearth of knowledge about the phenological behavior and long-term changes that these forests are experiencing. Thus, this study reports on leaf area seasonality and its time trend over the past two decades as assessed from multiple remotely sensed datasets. Seasonal variations of leaf area in Congolese forests derived from MODIS data co-vary with the bimodal precipitation pattern in this region, with higher values during the wet season. Independent observational evidence derived from MISR and EPIC sensors in the form of angular reflectance signatures further corroborate this seasonal behavior of leaf area. The bimodal patterns vary latitudinally within this large region. Two sub-seasonal cycles, each consisting of a dry and wet season, could be discerned clearly. These exhibit different sensitivities to changes in precipitation. Contrary to a previous published report, no widespread decline in leaf area was detected across the entire extent of the Congolese rainforests over the past two decades with the latest MODIS Collection 6 dataset. Long-term precipitation decline did occur in some localized areas, but these had minimal impacts on leaf area, as inferred from MODIS and MISR multi-angle observations.

Keywords: leaf area, remote sensing, Congolese rainforests, phenology, long-term trends, MODIS, MISR, DSCOVR EPIC

1. Introduction

Tropical rainforests play an essential role in modulating regional climate, surface energy partitioning and the Earth's carbon cycle (Chen et al. 2020; Cook et al. 2020). Understanding the spatial patterns and temporal variations and trends in the structure and functioning of rainforests, and the underlying mechanisms and their drivers, is crucial to gaining insights on how these biodiversly-rich and productive ecosystems will respond to future climate change, disturbances and human appropriation (Bi et al. 2015). The seasonal transition between wet and dry seasons is a distinct feature of tropical rainforests, which leads to intra-annual patterns of leaf flushing and abscission (Bi et al. 2015; Samanta et al. 2012). The growth-limiting impact of water deficit on rainforest during the dry season could be alleviated through deep roots and hydraulic redistribution (Oliveira et al. 2005; Pierret et al. 2016). However, a continued decline in leaf area and photosynthetic capacity attributed to long-term drying may alter forest composition and structure, such as large-scale tree mortality and dominance of drought-tolerant species (Adams et al. 2009; Fauset et al. 2012; Martínez-Vilalta and Lloret 2016).

Seasonal variations in the Amazonian rainforests has been an active research topic in recent years (Brando et al. 2010; Huete et al. 2006; Morton et al. 2014; Myneni et al. 2007). The community-consensual view is that higher greenness and leaf area appear during the sunlight-rich dry season in well-hydrated Amazonian rainforests (Bi et al. 2015; Brando et al. 2010; Huete et al. 2006; Myneni et al. 2007), even though this view has been questioned (Galvão et al. 2011; Morton et al. 2014). Science questions surrounding the functionality of Amazonian rainforests such as drought induced carbon sink variation and impacts of human interference are at the center of debates nowadays (Aragão et al. 2018; Brienen et al. 2015; Pires and Costa 2013; Yang et al. 2018b). The equatorial rainforests of Central Africa, the second largest and least disturbed of the biodiversly-rich and highly productive rainforests on Earth (Cook et al. 2020), have attracted less attention compared with its Amazonian counterpart.

The bimodal precipitation pattern (two wet and two dry seasons per year) in the Congo basin controlled by the migration of the tropical rain belt, is much different from that in the Amazon (Jiang et al. 2019; Nicholson 2018; Raghavendra et al. 2020; Sorí et al. 2017). For all vegetation types within the Congo Basin enhanced vegetation index (EVI) profiles were found to be highly

seasonal and strongly correlated to rainfall and to a lesser extent to light regimes (Gond et al. 2013). Two-band enhanced vegetation index (EVI2) from the geostationary Spinning Enhanced Visible and Infrared Imager (SEVIRI) and polar-orbiting Moderate Resolution Imaging Spectroradiometer (MODIS) also revealed similar bimodal seasonal pattern (Yan et al. 2016a). It was found (Yan et al. 2017) that the spatial variation in wet season timing within the Congo Basin exhibited distinct latitudinal gradients whereas the variation in the canopy greenness cycle timing was relatively small. Analyses of MODIS EVI and solar-induced chlorophyll fluorescence (SIF) and fraction of absorbed radiation from the Global Ozone Monitoring Experiment-2 (GOME-2) suggest that an annual rainfall threshold of approximately 2000 mm yr^{-1} determines whether the supply of seasonally redistributed subsurface water storage from the wet season can satisfy plant water demands in the subsequent dry season; thus water availability exerts a first-order control on photosynthetic seasonality in tropical forests (Guan et al. 2015; Ndehedehe et al. 2019).

Recent studies have also revealed a large-scale and long-term drying trend during the 1979 to 2010 period over the Congolese rainforests in central Africa (Jiang et al. 2019; Raghavendra et al. 2020; Zhou et al. 2014). This has been linked to a shift in tropical Walker circulation (Hua et al. 2018; Hua et al. 2016), intensifying thunderstorm activities (Raghavendra et al. 2018) and Madden-Julian oscillation (Raghavendra et al. 2020). This drying was supposed to have led to a widespread loss in greenness of Congolese forests during 2000 to 2012 as they were claimed to be more sensitive and less resilient to climate change as compared to its Amazonian counterpart (Hirota et al. 2011; Jiang et al. 2019; Zhou et al. 2014) . On the other hand, some recent studies based on latest versions of satellite data reported no significant browning signals during the 2000 to 2017 period (Chen et al. 2019; Piao et al. 2020). As such, the question of greening or browning of Congolese rainforests over the past 20 years is still unclear and in debate, especially in the context of increasing drying durations and from the perspective of biophysical parameters. Moreover, a drying climate over the past two decades has been associated with changes in forest composition, leaf phenology and community-level functional traits in tropical forests (Aguirre-Gutiérrez et al. 2020), which requires further explorations.

In addition to climatic factors mentioned above, degradational transitions in land cover and agricultural expansion also drive the vegetation dynamics in rainforests (Costa et al. 2007). Since

98 the Congolese rainforests are less disturbed by human activities compared with other equatorial
99 forests (Cook et al. 2020), the climatic influence is our main focus. This study is focused on
100 exploring the intra-annual seasonality and its controls, inter-annual variability and long-term
101 trends in leaf area of the Congolese rainforests. More specifically, our primary objectives are to (*i*)
102 document seasonal variation in leaf area of Congolese rainforests and how do seasonal patterns
103 vary latitudinally within this large region; (*ii*) estimate the sensitivity of leaf area to changes in
104 precipitation for different regions and seasonal cycles; (*iii*) analyze long-term trends in leaf area;
105 and (*iv*) assess impact of long-term drying on leaf area and leaf optics. Multiple remote sensing
106 datasets and vegetation proxy metrics are analyzed to achieve our objectives.
107
108 Monitoring of dense vegetation such as equatorial rainforests represents one of the most
109 complicated case in optical remote sensing because reflection of solar radiation saturates and
110 becomes weakly sensitive to vegetation changes. At the same time, the satellite data are strongly
111 influenced by changing sun-sensor geometry. This makes it difficult to discriminate between
112 vegetation changes and sun-sensor geometry effects. As such, the above-mentioned leaf area
113 seasonal variation and long-term greening/browning trends revealed by single-viewing remotely
114 sensed datasets require more evidence. Our secondary objective is to demonstrate value of multi-
115 angle observations to unambiguously detect changes in properties of dense equatorial forests.
116

117 ## 2. Materials and Methods

118

119 ### 2.1 Datasets

120 Various variables from several independent satellite sensors over the Congo basin were
121 analyzed in this research. These include leaf area index (LAI), normalized difference vegetation
122 index (NDVI) (Rouse et al. 1974), EVI (Liu and Huete 1995), land cover maps, land surface
123 temperature (LST) and evapotranspiration (ET) from MODIS. Additionally, the following datasets
124 were also utilized in this research: precipitation from Tropical Rainfall Measuring Mission
125 (TRMM), photosynthetically active radiation (PAR) from Clouds and Earth's Radiant Energy
126 System (CERES), surface bidirectional reflectance factor (BRF) and directional hemispherical
127 reflectance (DHR) from Multi-angle Imaging SpectroRadiometer (MISR) on the Terra platform

and BRF from Earth Polychromatic Imaging Camera (EPIC) on Deep Space Climate Observatory (DSCOVR). Table 1 shows datasets used in this study.

2.1.1. MODIS data

The Terra and Aqua MODIS Collection 6 (C6) 8-day composite LAI products (MOD15A2H and MYD15A2H) for the period of February 2000 to December 2019 were used in this study. The data are at 8-day temporal frequency and projected on a 500-m sinusoidal grid. The C6 MODIS LAI product correctly accommodates structural and phenological variability in all biome types and agree with ground truth data within root mean square error (RMSE) of 0.66 LAI (Yan et al. 2016b; Yan et al. 2016c).

C6 Terra MODIS monthly NDVI and EVI products (MOD13C2) from February 2000 to December 2019 were also used as radiometric measures of vegetation greenness. The NDVI is a vegetation index widely used in many studies of vegetation dynamic. It is calculated as the difference between BRFs at near-infrared (NIR) and red spectral bands normalized by their sum. The EVI is calculated as the difference between BRFs at NIR and red spectral bands normalized by a linear combination of BRFs at blue, red and NIR bands. It was found especially useful for monitoring vegetation in high biomass tropical broadleaf forests (Brando et al. 2010; Xu et al. 2011; Zhou et al. 2014). The C6 MOD13C2 product is projected on a 0.05° geographic Climate Modelling Grid (CMG) (Huete et al. 2002). In addition, monthly gridded Collection 5 (C5) MODIS NDVI/EVI product (MODVI) from February 2000 to December 2012 in CMG 1° resolution was also used in our study for comparisons.

C6 Terra and Aqua MODIS land cover product (MCD12C1) from 2001 to 2019 at yearly intervals and at a 0.05° spatial resolution was used to identify our study area. Maps of several classification schemes are available in the MCD12C1 dataset (Friedl et al. 2002). The map of LAI classification scheme was adopted in this research (Supplementary Information Figure S1).

Daytime LST from C6 Aqua MODIS (MYD11C3) for the period July 2002 to December 2019 was used to quantify temperature variations related to changes in leaf area and other climate variables. MYD11C3 measures the temperature of Earth's surface thermal emission at local time

~13:30, which is believed to provide the largest LST contrast between vegetated and non-vegetated surfaces compared to other MODIS LST measurements. Monthly LST values from the MYD11C3 product are derived by compositing and averaging values from the corresponding month of MYD11C1 daily files, and projected on a 0.05° CMG grid (Wan 2014).

The Terra MODIS C6 8-day composite evapotranspiration product (MOD16A2) projected on a 500-m sinusoidal grid from January 2000 to December 2019 was used to quantify climatic water deficit variations. The algorithm used to generate MOD16A2 is based on the logic of the Penman-Monteith equation, which includes inputs of daily meteorological reanalysis data along with other MODIS products such as vegetation property dynamics, albedo, and land cover (Mu et al. 2007; Mu et al. 2011).

2.1.2. TRMM Precipitation and CERES PAR Fluxes

Monthly precipitation data from the TRMM (3B43 version 7) at 0.25° spatial resolution for the period January 2000 to December 2019 was used in this study. The 3B43 version 7 TRMM data provides the best-estimate precipitation rate and root-mean-square precipitation-error estimates by combining four independent precipitation fields (Huffman et al. 2007). Monthly at-surface all-sky downward PAR, calculated by summarizing direct and diffuse PAR fluxes from CERES (SYN1deg_L3 product) at 1° resolution for the period of March 2000 to November 2019 was used (Rutan et al. 2015).

2.1.3. Terra MISR and DSCOVR EPIC data

Level 2 land surface and aerosol products from MISR (version 3) for the period of January 2000 to December 2019 were used in this study. The MISR sensor views the Earth's surface with nine cameras simultaneously and enables direct measurements of angular variation of forest reflected radiation over a wide range of the phase angle that the single-viewing sensors (e.g., Terra and Aqua MODIS) can provide only in very limited cases (Bi et al. 2015; Song et al. 2018). MISR has a ground track repeat cycle every 16 days and achieves global coverage every 9 days. The surface reflectances, DHR and BRF, are at 1.1 km spatial resolution. The aerosol optical depth (AOD) is available at 4.4 km spatial resolution. The surface and aerosol products are projected on

189 Space Oblique Mercator (SOM) projection, in which the reference meridian nominally follows the
190 spacecraft ground track. The land surface product provides BRF at nine MISR view angles (nadir,
191 ±26.1°, ±45.6°, ±60.0° and ±70.5°) in four spectral bands (446, 558, 672, and 866 nm). The MISR
192 view directions form "view" lines on the polar plane (Supplementary Information Figure S2). Each
193 view line sees a certain part of the MISR 360 km swath.
194
195 Level 2 Multi-Angle Implementation of Atmospheric Correction (MAIAC) surface BRF
196 retrieved from DSCOVR EPIC observations from 2016 to 2019 was also used. The EPIC
197 instrument provides imageries in near backscattering directions with the phase angle between 4°
198 and 12° at ten ultra-violet to NIR narrow spectral bands. This feature complements MISR
199 observations since it extends MISR angular sampling to the near backscattering directions. The
200 MAIAC BRF are available at four spectral bands; they are 443, 551, 680 and 780 nm. Data are
201 projected on a 10-km sinusoidal grid and available at 65 to 110 min temporal frequency.
202
203 **2.2. Data processing**
204 This study was focused on structurally intact and undisturbed region of Congolese tropical
205 moist broadleaf forests in Central Africa (5°N-6°S, 14°E-31°E), which were defined as a region
206 with no changes in land cover type during the 2000 to 2019 period. First, evergreen broadleaf
207 forest pixels in the LAI classification scheme at 0.05° resolution for which no land use/cover
208 change was detected during the 2000 to 2019 period were selected. Second, the binary 0.05°
209 evergreen broadleaf forest images were spatially aggregated into a 0.25° coarser resolution map to
210 match the spatial resolution of rainfall TRMM dataset. Pixels at 0.25° resolution were labeled as
211 rainforest only if at least 80% of its 0.05° sub-pixels (i.e., 20 in 25 sub-pixels) were forested. Third,
212 those isolated pixels in the Congolese forest border were removed at 0.25° mask map to minimize
213 human impact. The 1,653 pixels at 0.25° resolution identified by this procedure were considered
214 as structurally intact and undisturbed forests.
215
216 All vegetation and climate variables were selected using flags indicating highest retrieval
217 quality. The 8-day 500 m LAI products from Terra (MOD15A2H) and Aqua (MYD15A2H)
218 MODIS sensors were used to generate monthly average LAI values. The cloud contaminated
219 pixels were removed. Only the best quality LAI values generated using main algorithm were used

in our analyses. The monthly LAIs were then spatially aggregated onto a 0.05° CMG grid (Chen et al. 2019). The evapotranspiration data used in our study was generated by selecting best-quality retrievals in the MODIS C6 ET product first and then degraded to 0.05° CMG monthly composites following the same procedure used to obtain LAI dataset. The LAI and NDVI/EVI were further refined by removing low quality data by consulting NDVI/EVI quality assurance (QA) flags. We selected highest quality LST based on LST QA. The LAI, NDVI/EVI, ET and LST datasets over intact and undisturbed region of the Congolese forests were then spatially aggregated to 0.25° resolution. During the process of spatial aggregation, only pixel whose sub-pixels are all valid was retained. Climatic water deficit (CWD) was calculated as the difference between potential evapotranspiration and actual evapotranspiration from the ET dataset. Nearest neighbor interpolation was adopted to resample data to 0.25° for the C5 NDVI/EVI and CERES PAR dataset at a spatial resolution coarser than 0.25°.

The MISR surface BRF and DHR were first refined by removing pixels with AOD over 0.3. EPIC images at local solar time around 10:30 am were used in our analyses, which were also refined by removing pixels with AOD over 0.3. MISR and EPIC datasets were further re-projected to 0.01° and 0.1° CMG grids, respectively. We expressed BRF and DHR values in a coordinate system with the polar axis pointed towards the Sun. The view zenith angle in this "sun-tracking" coordinates was given by the phase angle, γ, i.e. the angle between the directions to the sun and sensor and calculated as

$$\gamma = \mathrm{acos}[\cos SZA \cos VZA + \sin SZA \sin VZA \cos(SAA - VAA)] \quad (1)$$

where SZA, VZA, SAA, VAA are solar zenith angle, view zenith angle, solar azimuthal angle and view azimuthal angles (Bi et al. 2015). We assigned the sign "plus" to the phase angle if the direction to the MISR sensor approached the direction to sun from North, and "minus" otherwise (Supplementary Information Figure S2). In our sun-tracking coordinate system, the MISR BRF was a function of SZA, phase angle and MISR view line, the latter specified by VZA of the MISR nadir camera.

Monthly BRFs and DHRs accumulated over the 20-year period (2000 to 2019) were used to analyze seasonal variation of forest canopy reflectance. For each month, a median BRF value at each phase angle was calculated using all 20-year (2000 to 2019) valid observations of a given pixel in our study area. Histograms of valid MISR spectral DHR at each SZA accumulated over the 20-year period (2000 to 2019) were calculated for each pixel. The most probable values were used to represent spectral DHR of regions as a function of SZA. For analysis of interannual changes, we used median BRFs over the period of 2000-2002 and 2017-2019 to represent the start and the end period, respectively.

2.3. Interpretation of forest BRF

Reflectance of dense vegetation such as the Congolese forests saturates and becomes weakly sensitive to vegetation changes. At the same time, the satellite data are strongly influenced by changing sun-sensor geometry. This makes it difficult to discriminate between vegetation changes and effects of sun-sensor geometry. This section provides an overview of a new approach to detect changed in properties of dense vegetation using angular distribution of forest reflected radiation as a source of diagnostic information. This methodology will be used in Section 3.1 and Section 3.4 to corroborate seasonal and long-term variation in leaf area.

In the case of vegetation canopies with a dark background or sufficiently dense vegetation where the impact of the canopy background is negligible, the BRF can be approximated as (Knyazikhin et al. 2013):

$$\mathrm{BRF}_\lambda(\Omega_0, \Omega) = \frac{\rho(\Omega_0, \Omega) i_0}{1-p} \times \frac{\omega_\lambda (1-p)}{1-p\omega_\lambda} \quad (2)$$

The first factor on the right-hand side of Eq (2), $\rho(\Omega_0, \Omega) i_0/(1-p)$, is the Directional Area Scattering Factor (DASF), which describes the canopy BRF if the foliage does not absorb radiation. The second factor, $\omega_\lambda(1-p)/(1-p\omega_\lambda)$, is the Canopy Scattering Coefficient (CSC), i.e., the fraction of intercepted radiation that has been reflected from, or diffusively transmitted through, the vegetation. Unlike canopy reflectance and transmittance, the CSC quantifies scattering event per unit leaf surface and therefore conveys information about leaf optical

properties. Here $\Omega_0 \sim (\mathrm{SZA}, \mathrm{SAA})$ and $\Omega \sim (\mathrm{VZA}, \mathrm{VAA})$ are unit vectors directed from target to the sun and sensor, respectively; i_0 is the canopy interceptance defined as the portion of photons from the incident solar beam that collide with foliage elements for the first time. The symbol ρ designates the directional escape probability, i.e., the probability by which a photon scattered by a foliage element will exit the vegetation in the direction Ω through gaps. Spherical integration of $\pi^{-1}\rho \cdot cos(VZA)$ results in $1 - p$, where p is the recollision probability, defined as the probability that a photon scattered by a foliage element in the canopy will interact within the canopy again (Yang et al. 2017). Finally, ω_λ is the wavelength dependent leaf albedo, i.e., the fraction of radiation incident on a leaf surface that is reflected or transmitted (Huang et al. 2007; Knyazikhin et al. 2011; Wang et al. 2003). We used Eq. (2) to interpret the BRF of Congolese forests. A short summary of its key properties is given below.

The spectrally invariant DASF is a function of canopy geometrical properties, such as the tree crown shape and size, spatial distribution of trees on the ground, and within-crown foliage arrangement (Knyazikhin et al. 2013). Since our study is focused on structurally intact and undisturbed region of the Congolese forests (i.e., no changes in forest geometry), only variation in leaf area can cause variation in DASF. At a given SZA, DASF increases with LAI in all phase angles. At a given LAI, the DASF exhibits a sharp increase as phase angle tends to zero and reaches its maximum value in the retro-illumination direction. This phenomenon is known as the hot spot effect. Increasing SZA with constant LAI results in an asymmetric transformation of the DASF, i.e., increase in its magnitude in backscattering directions, and changes in the range of DASF variations for positive and negative phase angles. This asymmetric transformation also can cause the two DASF signatures to intersect. More details about the effects of changing SZA and LAI on BRF can be found in (Bi et al. 2015).

The spectrally varying CSC is a function of the recollision probability and leaf optics. It increases with the leaf albedo: the more the leaves scatter, the brighter the canopy. As the recollision probability increases with LAI, an increase in LAI triggers an opposite tendency: more photon-foliage interactions and consequently a higher chance for photon to be absorbed. This tends to lower CSC. Such variations trigger a competing process: increase in LAI tends to darken the vegetation while increase in leaf albedo suppresses it. Note that DASF increases with LAI. This

not only compensates for a decrease in the CSC but also makes the BRF an increasing function with respect to leaf albedo and LAI.

The leaf albedo is close to unity, $\omega_\lambda \sim 1$ at weakly absorbing wavelengths such as NIR. In the case of dense vegetation, the recollision probability saturates and become weakly sensitive to LAI. In many instances, variation in LAI with leaf albedo unchanged cannot explain the magnitude of observed variation in CSC under the reflectance saturation conditions. Leaf albedo becomes a key parameter that controls changes in the CSC. A detailed mathematical analysis of variation in the CSC when LAI and leaf albedo vary simultaneously can be found in (Samanta et al. 2012).

The leaf albedo is close to zero, $\omega_\lambda \sim 0$ at strongly absorbing wavelengths. The contribution of multiple scattered photons to BRF and CSC is negligible. A decrease in LAI while holding leaf optics constant necessarily causes a decrease in BRF. The lack of BRF decrease indicates an increase in leaf albedo. Clearly this is also true for DHR, which is just hemispherically integrated BRF. We will use this property to detect changes in leaf albedo.

We followed a methodology documented in (Marshak and Knyazikhin 2017; Song et al. 2018) to approximate DASF. In this approach, the green and NIR wavelengths are used. Given the BRF at these two wavelengths, the estimate DASF is as:

$$\mathrm{DASF} = \frac{\mathrm{BRF}_{\mathrm{green}}\mathrm{BRF}_{\mathrm{NIR}}}{\mathrm{BRF}_{\mathrm{green}} - \beta(\mathrm{BRF}_{\mathrm{NIR}} - \mathrm{BRF}_{\mathrm{green}})}. \quad (3)$$

Here $\mathrm{BRF}_{\mathrm{green}}$ and $\mathrm{BRF}_{\mathrm{NIR}}$ are BRF at green and NIR wavelengths, $\beta = (1 - \omega_{\mathrm{NIR}})\omega_{\mathrm{green}}/(\omega_{\mathrm{NIR}} - \omega_{\mathrm{green}})$, and ω_{green} and ω_{NIR} stand for leaf albedo at green and NIR spectral bands. DASF defined by Eq. (3) does not vary with variation in ω_{green} and ω_{nir} as long as canopy structure remains unchanged. We used the leaf level albedo of the brightest leaf, whose values at green and NIR spectral bands were $\omega_{555} = 0.472$, $\omega_{865} = 0.978$ for MISR and $\omega_{551} = 0.490$, $\omega_{779} = 0.979$ for EPIC. These values were obtained from Lewis and Disney's approximation (Lewis and Disney 2007) of the PROSPECT model (Féret et al. 2008) with the following parameters: chlorophyll content of 16 μg cm^{-2}; equivalent water thickness of 0.005 cm^{-1}, and dry

matter content of 0.002 g cm^{-1}. It was shown that retrieval of DASF using this methodology is weakly sensitive to the uncertainties in the spectral properties of the atmospheric optical depth above the canopy, and the spectral CSC is very sensitive to the presence of chlorophyll in the scene (Marshak and Knyazikhin 2017).

2.4. Correlation and trends analysis

Correlation of monthly average leaf area and the corresponding climatic variables (e.g., precipitation, PAR) was assessed using Pearson's correlation coefficient. Trends in seasonal average variables (e.g., LAI) for the period of 2000 to 2012 and 2000 to 2019 were evaluated by ordinary least square (OLS) regression test using noise-removed dataset, and the trends with $P \leq 0.1$ were considered as statistically significant in this study to make our results comparable with those reported in (Zhou et al. 2014).

3. Results

3.1. Seasonal variation of leaf area and leaf optics

Monthly precipitation data over the Congolese forests show a bimodal variation that suggests two wet and two dry seasons during the year. It varies between its maximum of about 219 mm in October and the minimum of about 86 mm in January (Figure 1). The wet seasons occur in March-April-May (MAM, wet season 1) and September-October-November (SON, wet season 2), while dry season months are December-January-February (DJF, dry season 1) and June-July-August (JJA, dry season 2) (Figure 1 and Supplementary Information Figure S3a). The PAR data exhibit a quasi-bimodal pattern, although somewhat less distinctly: clear-cut variations from December to October and a weak oscillation from October to December (Figure 1 and Supplementary Information Figure S3). The sub-seasonal cycle 1 from December to May (dry season 1 and wet season 1) shows less precipitation and more PAR, while cycle 2 from June to December has more precipitation and less PAR (Figure 1 and Supplementary Information Figure S3). Monthly average LAI and EPIC NIR BRF data over the Congolese forests also exhibit notable bimodal seasonal variations, which follow the patterns of precipitation (Figure 1 and Supplementary Information Figure S3a and b). LAI varies between its maximum of about 5.7 during the wet seasons and a dry season minimum of about 4.6.

Congolese forests can be further divided into four phenological regions based on normalized 20-year mean monthly climatology of precipitation, PAR and LAI using a K-means clustering method, which is an unsupervised measure to find similar features from multiple inputs (Celik 2009; Xu et al. 2015). We use the four-cluster partition in this study because clusters are big enough to accumulate valid data for statistical analyses and their respective homogeneities are preserved (Figure 2). Other numbers of clusters are also tested to find an optimal partitioning, and all clusters were generally parallel to the Equator (Supplementary Information Figure S4), likely because the seasonality of these forests is mainly controlled by the migration of the tropical rain belt and variation of solar radiation along the latitude. Distinct seasonal patterns of climatic and vegetation variables are clearly seen in all phenological regions across the Congo Basin (Figure 3). The amplitude of all variables tends to increase from region 1 (north) to region 3 (south) between March and October, which makes the bimodality more distinct. The highland forest (region 4) is characterized by lower LAI values and higher rainfall compared to its lowland counterparts, which is typical of montane forests. The EPIC sensor likely sees different slopes of the mountains; hence the NIR BRF is somewhat less synchronized with LAI compared to other regions. We exclude this region from further analyses given its smaller areal extent and specific character.

Spectrally invariant DASF is a function of canopy geometrical properties, such as the tree crown shape and size, and leaf area density within the canopy. The DASF derived from MISR and EPIC observations of selected regions during wet and dry seasons are different (Figure 4, left Panels), showing a districting decrease in all directions from wet (October, November) to dry (January) seasons. Such a downward shift in DASF can only result from a negative change in LAI because other structural variables, such as tree crown shape and size do not vary seasonally in our forests. BRF at NIR spectral band exhibits similar behavior: a decrease in reflected radiation in all directions from October (November) to January (Supplementary Information Figure S5), which suggests more green leaves during the wet season. The CSC shows an opposite tendency, i.e., a positive increase between wet and dry seasons at all spectral bands (Figure 4, right panels). The decline in LAI is one reason for the observed increase (Section 2.3). A change in leaf albedo is another reason that can impact this coefficient (Section 2.3). Decrease in leaf albedo lowers the

399 CSC value whereas its increase results in the positive change of the CSC value. The question then
400 arises whether one can detect changes in the leaf albedo given changes in the CSC.
401
402 A reduction of leaf area tends to decrease forest canopy reflectance (BRF and consequently
403 DHR). At strongly absorbing red (672 nm) wavelength, however, the DHR has increased between
404 wet and dry seasons from 0.014 to about 0.024 in regions 1 and 2 and from 0.015 to 0.018 in region
405 3 (Figure 4, left panels). This increase in DHR with decreasing LAI necessarily indicates an
406 increase in leaf albedo (Section 2.3). This also takes place for strongly absorbing blue (446 nm)
407 and moderately absorbing green (551 nm) wavelengths: no decrease in DHR from wet to dry
408 season. This suggests an increase in leaf albedo at visible spectral bands. At NIR (866 nm)
409 wavelength, forest canopy reflectance and CSC show opposite tendencies, namely, BRF (and
410 DHR) decrease whereas CSC increases between wet and dry seasons. Similar tendencies were
411 documented for the Amazonian rainforests (Köhler et al. 2018) and for sufficiently dense broad-
412 and needleleaf forests in the USA (Knyazikhin et al. 2013). A decrease in LAI (and consequently,
413 the recollision probability) tends to increase the CSC (Section 2.3). Under saturation conditions,
414 however, the change in the recollision probability is negligible. The observed variation in CSC is
415 therefore likely due to a positive change in the leaf albedo.
416
417 The sensitivity analyses based on the PROSAIL model (Jacquemoud et al. 2009) suggest that
418 under saturation conditions (LAI>4), the scattering coefficient is nearly insensitive to variations in
419 LAI and SZA (Supplementary Information Figure S6, panels a and b). The observed changes in
420 the CSC between wet and dry seasons therefore are not due variation in LAI and SZA. In the
421 spectral interval between 450 nm and about 750 nm, chlorophyll is the dominant pigment that
422 absorbs radiation primarily in the blue and red regions of the spectrum, less in in the green and
423 essentially none in NIR. This feature makes the CSC sensitive to its concentration in the green and
424 flat in NIR spectral bands (Supplementary Information Figure S6, panel c). The chlorophyll
425 absorption spectrum declines rapidly with wavelength near the red spectral region and vanishes at
426 about 770 nm, resulting in a sharp jump in the spectrum of leaf albedo from its minimum to a
427 plateau around 800 nm. The magnitude of this plateau is controlled by the amount of dry matter.
428 This imparts sensitivity of the NIR CSC to the concentration of dry matter (Supplementary
429 Information Figure S6, plot d).

In summary, seasonal variation of leaf area in Congolese forests co-varies with the bimodal precipitation pattern, with higher values during the wet seasons. The bimodal pattern is different in the three identified regions, with its bimodality more distinct from the south to the north. The canopy scattering coefficient exhibits an opposite tendency: its value increases from wet to dry and decreases from dry to wet seasons. These variations can be linked to variation in the concentrations of chlorophyll and/or dry matter in green leaves.

3.2. Sensitivity of leaf area to changes in precipitation

Pearson's correlation coefficients between monthly average precipitation, PAR and LAI for the identified regions (Figure 2) and seasonal periods are shown in Table 2. With the exception of region 3 and seasonal cycle 1, a significant positive correlation between precipitation and LAI is observed. Moreover, the time series of 20-year monthly precipitation and LAI over the Congolese forests are also significantly positively correlated (R=0.67, P<0.01, Supplementary Information Figure S7). Such correlations between LAI and PAR (P<0.01) are found in regions 1 to 3 during the cycle 2 (June through November) and in region 3 during the cycle 1 (December through May). These variables are negatively correlated (P<0.1) in region 1 during cycle 1 (Table 2).

We estimate the sensitivity, $\Delta LAI/\Delta precipitation$, of monthly LAI to changes in precipitation for different regions and seasonal cycles using the slopes of linear regressions. The overall sensitivity of LAI to changes in precipitation varies between regions and depends on the seasonal cycle. It tends to decrease from north to south for the full seasonal cycle (December to November) (Figure 5a). The regions show weak variation of the sensitivity within seasonal cycles (cf. Figure 5b and 5c). LAI exhibits a stronger response to changes in the precipitation during the seasonal cycle 1 (December to June). This difference is due to very different distributions of precipitation, PAR and climatic water deficit during cycles 1 and 2 (Supplementary Information Figure S8). More precipitation occurs in cycle 2 than in cycle 1, causing a higher climatic water deficit. Thus, LAI in our forests is more sensitive to the changes in precipitation during cycle 1.

3.3. Long-term trends in leaf area

A widespread decline in Congolese rainforest greenness over the 2000-2012 period has been recently reported (Jiang et al. 2019; Raghavendra et al. 2020; Zhou et al. 2014). This result however was questioned, suggesting no significant browning signal in the 2000 to 2017 period (Chen et al. 2019; Piao et al. 2020). These contradictory results justify a re-examination of the long-term trend in greenness of the Congolese forests. Here, we reproduce linear trends in C5 EVI and precipitation in April-May-June for the 2000 to 2012 period as reported in (Zhou et al. 2014) and for an extended period of 2000 to 2019 first, and then generate linear trends in C6 EVI, NDVI and LAI for the same periods.

The MODIS C5 EVI declines over 98% of the study area, with 54% showing a significant negative trend (P<0.1) (Figure 6a). TRMM precipitation declines over 77% of the area with 13% indicating significant change with P<0.1 (Figure 6b). These results suggest decrease in rainfall and widespread decline in Congo rainforest greenness from 2000 to 2012. Note that "drying area" is reduced from 77% to 63% (13% to 5% with P<0.1) for the period of 2000 to 2019.

The widespread decline of Congo rainforest greenness in the 2000 to 2012 period has disappeared in the latest Collection 6 MODIS data (Figure 6, middle panels). Our re-analyses suggest declines in EVI, NDVI and LAI over 43% to 51% of the study area with only 2% to 5% showing significant negative trends (P<0.1). For the longer period (2000 to 2019), the browning areas have been reduced to 19%-42%, with a negative trends below 4% (P<0.1) (Figure 6, lower panels). The difference in the trends is attributable to Terra MODIS sensor degradation found in C5 data (Wang et al. 2012; Zhang et al. 2017).

The regional mean precipitation and PAR over 20 years do not show significant positive or negative trends for all seasons across the Congo basin because of strong interannual variability (Supplementary Information Figure S9). The regional mean LAI, however, increases by 0.0865 (P=0.0168) per decade during wet season 1 (March to May) from 2000 to 2019 (Supplementary Information Figure S9b), and the leaf area trends are also positive but not significant for the other wet or dry seasons (Supplementary Information Figure S9a, c, d).

3.4. Impact of drying trends on leaf area and leaf optics

Here we focus on a South-East part (0.5°N-2.5°S, 25.5°E-28.5°E) of our study area, where a significant precipitation decline is observed (Figures 7a and b), with the goal of understanding the impact of this event on changes in forest structure and leaf optics.

With the exception of NDVI in the dry season 2 (June to August), no significant decline or increase in trends in regional mean NDVI, EVI and LAI over the past two decades are detected. The time series of LAI and EVI are found to be strongly correlated with R=0.56 (P<0.01) in wet season 1 (MAM) and R=0.74 (P<0.01) in dry season 2 (JJA).

Next, we examine MISR BRFs at NIR (866 nm) spectral band over the region with significant drying happened during the early (2000-2002) and later (2017-2019) part of the 20-year observation period. Reflectance in April (wet season) and June (dry season) are under almost identical observation and illumination conditions (Figure 8 left panels). No significant differences in magnitude and shape of angular signatures of the reflected radiation at the beginning and the end of our observation period have been detected. Similarly, no changes in the canopy spectral coefficient at all MISR spectral bands are found. These findings suggest no changes in structure and leaf optics of the Congolese forests before and after the observed drying event. Thus we conclude, MODIS NDVI, EVI and LAI long-term records and MISR angular signatures of forest reflected radiation show no signs of long-term drying impact on structure and leaf optics of the Congolese forests.

4. Discussion

Tropical rainforests play an essential role in modulating regional climate, surface energy balance and the Earth's carbon cycle (Chen et al. 2020; Cook et al. 2020). Understanding the seasonal and long-term variations in the structure and function of these ecosystems is crucial to prognosing their response to climate change (Bi et al. 2015). The equatorial central African rainforests, the second-largest on Earth after the Amazonian rainforests, is still lacking systematic analyses of its phenological behavior and interannual variation. The purpose of this study is to analyze seasonal changes and long-term trends in leaf area in intact and undisturbed regions of the Congolese rainforests (Supplementary Information Figure S1) using remote sensing data from the past two decades. We focus on the analysis on three regions identified with normalized 20-year

mean monthly climatology of precipitation, PAR and LAI by using a K-means clustering algorithm, an unsupervised measure to find similar features from multiple inputs (Figure 2). This clustering technique also localizes a highland region in the southeast part (Region 4 in Figure 2) that represents a montane ecosystem.

Monthly precipitation data from TRMM show a bimodal variation over the Congolese rainforest, suggesting two dry (December-January-February and June-July-August) and two wet (September-October-November and March-April-May) seasons (Figure 3). This is consistent with other precipitation datasets, such as Global Precipitation Climatology Centre (GPCC), Global Precipitation Climatology Project (GPCP) and Climatic Research Unit (CRU) (Jiang et al. 2019; Raghavendra et al. 2020; Sorí et al. 2017). Monthly average LAI from MODIS and forest canopy reflectance from EPIC follow seasonal patterns of precipitation, with higher values during the wet seasons (Figure 3). The PAR incident on the forest canopy also exhibits a bimodal pattern, although somewhat less distinct: clear-cut variations from December to October and a weaker oscillation from October to December. Sub-seasonal cycle from December to May shows less precipitation and more PAR, while the cycle from June to December has more precipitation and less PAR (Figure 3). The bimodal patterns vary latitudinally with the amplitude increasing from North to South (Figure 3).

The MODIS LAI values used in this research are mostly retrieved under the condition of reflectance saturation. The seasonality of satellite data-based LAI may therefore result from a decreased retrieval accuracy and/or variation in sun-satellite sensor geometry (Galvão et al. 2011; Morton et al. 2014). We develop a new approach that allows us to unambiguously detect changes in properties of the Congolese rainforest using angular variation of forest BRF as a source of diagnostic information. This methodology is applied to obtained independent observational evidence from MISR and EPIC data in support of the validity of the satellite derived seasonal variation in leaf area. Angular variations of forest DASF and canopy reflectance observed by the MISR and EPIC sensors clearly show seasonal increases and decreases in the amount of radiation reflected by the Congolese forests in all directions simultaneously (Figure 4; Supplementary Information Figure S5). Such changes can only be attributed to corresponding seasonal increases and decreases of LAI. This corroborates the seasonal behavior of leaf area derived from the

MODIS observations. We also find that the canopy scattering coefficient exhibits an opposite tendency: its value increases from wet to dry and decreases from dry to wet seasons in the Congolese rainforests (Figure 4, right panels). Similar tendencies were also found in Amazonian rainforests (Köhler et al. 2018). Such variation can be linked to variation in the concentrations of chlorophyll and/or dry matter in green leaves (Supplementary Information Figure S6). In summary, our approach based on exploiting angular variation of forest reflected radiation as a source of diagnostic information, rooted in physics of radiative transfer, allows us to unambiguously detect changes in canopy structure and leaf optics. This undoubtedly offers the benefit of greater reliability of our conclusion.

A significant positive correlation between precipitation and LAI is observed for our study area and seasonal cycles (Table 2). The time series of 20-year monthly precipitation and LAI over the Congolese forests are significantly positively correlated (R=0.67, P<0.01, Figure S7). Whereas LAI and precipitation are always positively correlated, correlation between LAI and PAR can be both negative as during cycle 1 in regions 1 and 2 and positive as in cycle 2 (Table 2). These findings suggest that the observed seasonality of LAI is mainly controlled by precipitation in the Congolese rainforests (Gond et al. 2013; Yan et al. 2016a), as contrast to its Amazonian counterpart, where LAI is positive correlated with PAR (Bi et al. 2015; Brando et al. 2010; Huete et al. 2006; Myneni et al. 2007). Abundant annual precipitation (2,332 mm yr^{-1}) creates a well-hydrated environmental condition in the Amazonian rainforests (Yang et al. 2018a), thus the water is not a main limitation and higher leaf area appears during the sunlight-rich dry season. A decrease in annual precipitation (1,775 mm yr^{-1}) makes the leaf flushing and photosynthesis in the Congolese rainforests more dependent on water supply, especially in dry season when the monthly precipitation can fall below 90 mm (Figure 1). Less solar radiation during the dry season (Figure1 and Supplementary Information Figure S3) may lead to lower leaf area in the Congolese rainforests. This, however, can only explain LAI decrease in dry season 2 (JJA). In addition, a low-level cloudiness developing during the dry season 2 causes high quality of light that sustain a more efficient photosynthesis (Mercado et al. 2009; Philippon et al. 2019), which should benefits leaf area growing. Hence, water supply is believed as the main limitation for seasonal leaf area variation. From the ecological perspective, the difference in the total annual precipitation and its

583 diverse intra-annual variability strongly influence phenological behavior of rainforests and other
584 vegetation types in the tropical regions (Ndehedehe et al. 2019; Yan et al. 2017).
585
586 Distinct spatiotemporal dependence of leaf area sensitivity to the seasonal variation in
587 precipitation is observed in the Congo basin. The sensitivity of LAI to changes in precipitation
588 tends to decrease from north to south for the full seasonal cycle (December to November, Figure
589 5a). The phenological regions (Figure 2) show weak variations of the sensitivity within a seasonal
590 cycle (cf. Figure 5b and 5c). LAI exhibits a stronger response to changes in precipitation from
591 December to June compared to the second seasonal cycle (June to November). This difference is
592 attributed to very different distributions of precipitation, PAR and climatic water deficit during the
593 two seasonal cycles (Supplementary Information Figure S8). Note that only very few factors were
594 accounted for in our analyses. Further analyses of combined effects of precipitation, PAR, and
595 other factors are needed to obtain a comprehensive insight into the causes of leaf area seasonal
596 variation. Besides, a better understanding of the phenological response of Congolese rainforests
597 depends on further *in situ* studies as satellite data can only complement but not substitute field
598 data.
599
600 A widespread decline in Congolese rainforest greenness over the 2000-2012 period has been
601 recently reported (Jiang et al. 2019; Raghavendra et al. 2020; Zhou et al. 2014). This result
602 however was questioned, suggesting no significant browning signal in the 2000 to 2017 period
603 (Chen et al. 2019; Piao et al. 2020). These contradictory results justify a re-examination of the
604 long-term trend in greenness of the Congolese forests.
605
606 We reproduce their result using the same Terra MODIS C5 EVI data (Figure 6, upper panels),
607 which is then compared to that from the latest MODIS C6 EVI dataset. We find that the widespread
608 decline of Congo rainforest greenness disappear in the latest C6 MODIS data (Figure 6, middle
609 and lower panels): only 2% to 3% of the forests show significant negative trends in EVI, NDVI
610 and LAI ($P<0.1$) compared to 54% ($P<0.1$) decline in EVI reported in (Zhou et al. 2014). The
611 difference in the trends detected by C5 and C6 EVIs is attributed to the Terra MODIS sensor
612 degradation for the period after 2007 (Lyapustin et al. 2014; Wang et al. 2012; Zhang et al. 2017).
613 Moreover, a significant increase in total aerosols over the Congolese rainforests within the last

decade has been detected (Moparthy et al. 2019). This can amplify the apparent long-term trends of canopy greenness these changes in aerosol loads are not correctly taken into account. C6 data reprocessing has significantly alleviated these problems (Detsch et al. 2016; Zhang et al. 2017) and made the result more credible.

A significant precipitation decline has been observed in the South-East part of our study area (Figures 7a and b). However, no significant decline or increase in trends in regional mean NDVI, EVI and LAI over the past two decades are detected (Figures 7c and d). The time series of LAI and EVI are found to be strongly correlated with R=0.56 (P<0.01) during wet (March-April-May) and R=0.74 (P<0.01) during dry (June-July-August) seasons. We also find no significant differences in magnitude and shape of angular distribution of forest reflected radiation and leaf optics at the beginning and the end of our observation period (Figure 8). Thus, MODIS NDVI, EVI and LAI long-term records and MISR angular signatures of forest reflected radiation show no signs of drying impact on structure and leaf optics even in the South-East part of the Congolese forests where a significant drying is observed.

Long-term drying does not induce vegetation degradation, and possible explanations for the neutral response of leaf area to the declines in precipitations at the seasonal and inter-annual scales could be given as follows. First, the decrease in monthly precipitation under a long-term drying condition is much smaller compared to a wet-to-dry precipitation amplitude of about 219 mm to 86 mm (Figure 1), which still can satisfy plant water demands. Dry frequency is not high enough to suppress compensation of water supply from other months or seasons, allowing the forest to endure precipitation deficit. Second, decades of long-term drying in the Congolese rainforests may result in more drought-adapted species compared with other tropical forests, and this adaptive mechanisms by utilization of soil water reserves can tolerate water deficit short-time events (Asefi-Najafabady and Saatchi 2013; Borchert 1998). Third, suitable climate conditions—slight temperature increase and climatic water deficit decline (Supplementary Information Figure S10), may benefit the growth of vegetation (Li et al. 2019) and in turn offset the negative impact from precipitation decline. More comprehensive explorations, such as model-based study, on this debate are still needed in the future investigation to get a better understanding.

5. Conclusion

This study comprehensively evaluated the seasonality and long-term trends of leaf area in Congolese forests with multiple remotely sensed datasets. We found that the seasonal variations of leaf area from MODIS data co-vary with the bimodal precipitation pattern, with higher values during the wet season, and the bimodal patterns vary latitudinally within this large region. Angular reflectance signatures derived from MISR and EPIC data further corroborated this seasonal behavior of leaf area. Two sub-seasonal cycles, each consisting of a dry and wet season, exhibited different leaf area sensitivities to changes in precipitation. No widespread decline in leaf area was detected across the Congolese rainforest over the past two decades with the latest MODIS C6 dataset. Long-term drying did happen in some local areas of Congolese forests; however, those had minimal impacts on leaf area detected from MODIS and MISR observations.

Acknowledgment

This research was funded by grants from the Earth Science Division of the National Aeronautics and Space Administration. Yuanheng Sun was also funded by the Chinese Scholarship Council (201906010045).

References

Adams, H.D., Guardiola-Claramonte, M., Barron-Gafford, G.A., Villegas, J.C., Breshears, D.D., Zou, C.B., Troch, P.A., & Huxman, T.E. (2009). Temperature sensitivity of drought-induced tree mortality portends increased regional die-off under global-change-type drought. *Proceedings of the National Academy of Sciences, 106*, 7063-7066

Aguirre-Gutiérrez, J., Malhi, Y., Lewis, S.L., Fauset, S., Adu-Bredu, S., Affum-Baffoe, K., Baker, T.R., Gvozdevaite, A., Hubau, W., Moore, S., Peprah, T., Ziemińska, K., Phillips, O.L., & Oliveras, I. (2020). Long-term droughts may drive drier tropical forests towards increased functional, taxonomic and phylogenetic homogeneity. *Nature Communications, 11*, 3346

Aragão, L.E.O.C., Anderson, L.O., Fonseca, M.G., Rosan, T.M., Vedovato, L.B., Wagner, F.H., Silva, C.V.J., Silva Junior, C.H.L., Arai, E., Aguiar, A.P., Barlow, J., Berenguer, E., Deeter, M.N., Domingues, L.G., Gatti, L., Gloor, M., Malhi, Y., Marengo, J.A., Miller, J.B., Phillips, O.L., & Saatchi, S. (2018). 21st Century drought-related fires counteract the decline of Amazon deforestation carbon emissions. *Nature Communications, 9*, 536

Asefi-Najafabady, S., & Saatchi, S. (2013). Response of African humid tropical forests to recent rainfall anomalies. *Philosophical Transactions of the Royal Society B: Biological Sciences, 368*, 20120306

Bi, J., Knyazikhin, Y., Choi, S., Park, T., Barichivich, J., Ciais, P., Fu, R., Ganguly, S., Hall, F., Hilker, T., Huete, A., Jones, M., Kimball, J., Lyapustin, A.I., Mottus, M., Nemani, R.R., Piao, S., Poulter, B., Saleska, S.R., Saatchi, S.S., Xu, L., Zhou, L., & Myneni, R.B. (2015). Sunlight mediated seasonality in canopy structure and photosynthetic activity of Amazonian rainforests. *Environmental Research Letters, 10*

Borchert, R. (1998). Responses of Tropical Trees to Rainfall Seasonality and its Long-Term Changes. *Climatic Change, 39*, 381-393

Brando, P.M., Goetz, S.J., Baccini, A., Nepstad, D.C., Beck, P.S.A., & Christman, M.C. (2010). Seasonal and interannual variability of climate and vegetation indices across the Amazon. *Proceedings of the National Academy of Sciences, 107*, 14685-14690

Brienen, R.J.W., Phillips, O.L., Feldpausch, T.R., Gloor, E., Baker, T.R., Lloyd, J., Lopez-Gonzalez, G., Monteagudo-Mendoza, A., Malhi, Y., Lewis, S.L., Vásquez Martinez, R., Alexiades, M., Álvarez Dávila, E., Alvarez-Loayza, P., Andrade, A., Aragão, L.E.O.C., Araujo-Murakami, A., Arets, E.J.M.M., Arroyo, L., Aymard C, G.A., Bánki, O.S., Baraloto, C., Barroso, J., Bonal, D., Boot, R.G.A., Camargo, J.L.C., Castilho, C.V., Chama, V., Chao, K.J., Chave, J., Comiskey, J.A., Cornejo Valverde, F., da Costa, L., de Oliveira, E.A., Di Fiore, A., Erwin, T.L., Fauset, S., Forsthofer, M., Galbraith, D.R., Grahame, E.S., Groot, N., Hérault, B., Higuchi, N., Honorio Coronado, E.N., Keeling, H., Killeen, T.J., Laurance, W.F., Laurance, S., Licona, J., Magnussen, W.E., Marimon, B.S., Marimon-Junior, B.H., Mendoza, C., Neill, D.A., Nogueira, E.M., Núñez, P., Pallqui Camacho, N.C., Parada, A., Pardo-Molina, G., Peacock, J., Peña-Claros, M., Pickavance, G.C., Pitman, N.C.A., Poorter, L., Prieto, A., Quesada, C.A., Ramírez, F., Ramírez-Angulo, H., Restrepo, Z., Roopsind, A., Rudas, A., Salomão, R.P., Schwarz, M., Silva, N., Silva-Espejo, J.E.,

703 Silveira, M., Stropp, J., Talbot, J., ter Steege, H., Teran-Aguilar, J., Terborgh, J., Thomas-Caesar,
704 R., Toledo, M., Torello-Raventos, M., Umetsu, R.K., van der Heijden, G.M.F., van der Hout, P.,
705 Guimarães Vieira, I.C., Vieira, S.A., Vilanova, E., Vos, V.A., & Zagt, R.J. (2015). Long-term
706 decline of the Amazon carbon sink. *Nature, 519*, 344-348

707 Celik, T. (2009). Unsupervised Change Detection in Satellite Images Using Principal Component
708 Analysis and k-Means Clustering. *IEEE Geoscience and Remote Sensing Letters, 6*, 772-776

709 Chen, C., Li, D., Li, Y., Piao, S., Wang, X., Huang, M., Gentine, P., Nemani, R.R., & Myneni, R.B.
710 (2020). Biophysical impacts of Earth greening largely controlled by aerodynamic resistance.
711 *Science Advances, 6*, eabb1981

712 Chen, C., Park, T., Wang, X., Piao, S., Xu, B., Chaturvedi, R.K., Fuchs, R., Brovkin, V., Ciais, P.,
713 Fensholt, R., Tømmervik, H., Bala, G., Zhu, Z., Nemani, R.R., & Myneni, R.B. (2019). China and
714 India lead in greening of the world through land-use management. *Nature Sustainability, 2*, 122-
715 129

716 Cook, K.H., Liu, Y., & Vizy, E.K. (2020). Congo Basin drying associated with poleward shifts of
717 the African thermal lows. *Climate Dynamics, 54*, 863-883

718 Costa, M.H., Yanagi, S.N.M., Souza, P.J.O.P., Ribeiro, A., & Rocha, E.J.P. (2007). Climate change
719 in Amazonia caused by soybean cropland expansion, as compared to caused by pastureland
720 expansion. *Geophysical Research Letters, 34*

721 Detsch, F., Insa, O., Appelhans, T., & Nauss, T. (2016). A Comparative Study of Cross-Product
722 NDVI Dynamics in the Kilimanjaro Region—A Matter of Sensor, Degradation Calibration, and
723 Significance. *Remote Sensing, 8*

724 Fauset, S., Baker, T.R., Lewis, S.L., Feldpausch, T.R., Affum-Baffoe, K., Foli, E.G., Hamer, K.C.,
725 & Swaine, M.D. (2012). Drought-induced shifts in the floristic and functional composition of
726 tropical forests in Ghana. *Ecology Letters, 15*, 1120-1129

727 Féret, J.B., Francois, C., Asner, G.P., Gitelson, A.A., Martin, R.E., Bidel, L.P.R., Ustin, S.L., le
728 Maire, G., & Jacquemoud, S. (2008). PROSPECT-4 and 5: Advances in the leaf optical properties
729 model separating photosynthetic pigments. *Remote Sensing of Environment, 112*, 3030-3043

730 Friedl, M.A., McIver, D.K., Hodges, J.C.F., Zhang, X.Y., Muchoney, D., Strahler, A.H., Woodcock,
731 C.E., Gopal, S., Schneider, A., Cooper, A., Baccini, A., Gao, F., & Schaaf, C. (2002). Global land
732 cover mapping from MODIS: algorithms and early results. *Remote Sensing of Environment, 83*,
733 287-302

734 Galvão, L.S., dos Santos, J.R., Roberts, D.A., Breunig, F.M., Toomey, M., & de Moura, Y.M.
735 (2011). On intra-annual EVI variability in the dry season of tropical forest: A case study with
736 MODIS and hyperspectral data. *Remote Sensing of Environment, 115*, 2350-2359

737 Gond, V., Fayolle, A., Pennec, A., Cornu, G., Mayaux, P., Camberlin, P., Doumenge, C., Fauvet,
738 N., & Gourlet-Fleury, S. (2013). Vegetation structure and greenness in Central Africa from Modis
739 multi-temporal data. *Philosophical Transactions of the Royal Society B: Biological Sciences, 368*,

20120309

Guan, K., Pan, M., Li, H., Wolf, A., Wu, J., Medvigy, D., Caylor, K.K., Sheffield, J., Wood, E.F., Malhi, Y., Liang, M., Kimball, J.S., Saleska, Scott R., Berry, J., Joiner, J., & Lyapustin, A.I. (2015). Photosynthetic seasonality of global tropical forests constrained by hydroclimate. *Nature Geoscience, 8*, 284-289

Hirota, M., Holmgren, M., Van Nes, E.H., & Scheffer, M. (2011). Global Resilience of Tropical Forest and Savanna to Critical Transitions. *Science, 334*, 232-235

Hua, W., Zhou, L., Chen, H., Nicholson, S.E., Jiang, Y., & Raghavendra, A. (2018). Understanding the Central Equatorial African long-term drought using AMIP-type simulations. *Climate Dynamics, 50*, 1115-1128

Hua, W., Zhou, L., Chen, H., Nicholson, S.E., Raghavendra, A., & Jiang, Y. (2016). Possible causes of the Central Equatorial African long-term drought. *Environmental Research Letters, 11*, 124002

Huang, D., Knyazikhin, Y., Dickinson, R.E., Rautiainen, M., Stenberg, P., Disney, M., Lewis, P., Cescatti, A., Tian, Y., Verhoef, W., Martonchik, J.V., & Myneni, R.B. (2007). Canopy spectral invariants for remote sensing and model applications. *Remote Sensing of Environment, 106*, 106-122

Huete, A., Didan, K., Miura, T., Rodriguez, E.P., Gao, X., & Ferreira, L.G. (2002). Overview of the radiometric and biophysical performance of the MODIS vegetation indices. *Remote Sensing of Environment, 83*, 195-213

Huete, A.R., Didan, K., Shimabukuro, Y.E., Ratana, P., Saleska, S.R., Hutyra, L.R., Yang, W., Nemani, R.R., & Myneni, R. (2006). Amazon rainforests green-up with sunlight in dry season. *Geophysical Research Letters, 33*

Huffman, G.J., Bolvin, D.T., Nelkin, E.J., Wolff, D.B., Adler, R.F., Gu, G., Hong, Y., Bowman, K.P., & Stocker, E.F. (2007). The TRMM Multisatellite Precipitation Analysis (TMPA): Quasi-Global, Multiyear, Combined-Sensor Precipitation Estimates at Fine Scales. *Journal of Hydrometeorology, 8*, 38-55

Jacquemoud, S., Verhoef, W., Baret, F., Bacour, C., Zarco-Tejada, P.J., Asner, G.P., François, C., & Ustin, S.L. (2009). PROSPECT+SAIL models: A review of use for vegetation characterization. *Remote Sensing of Environment, 113*, S56-S66

Jiang, Y., Zhou, L., Tucker, C.J., Raghavendra, A., Hua, W., Liu, Y.Y., & Joiner, J. (2019). Widespread increase of boreal summer dry season length over the Congo rainforest. *Nature Climate Change, 9*, 617-+

Knyazikhin, Y., Schull, M., Xu, L., Myneni, R., & Samanta, A. (2011). Canopy spectral invariants. Part 1: A new concept in remote sensing of vegetation. *Journal of Quantitative Spectroscopy & Radiative Transfer, 112*, 727-735

Knyazikhin, Y., Schull, M.A., Stenberg, P., Mottus, M., Rautiainen, M., Yang, Y., Marshak, A.,

776 Latorre Carmona, P., Kaufmann, R.K., Lewis, P., Disney, M.I., Vanderbilt, V., Davis, A.B., Baret,
777 F., Jacquemoud, S., Lyapustin, A., & Myneni, R.B. (2013). Hyperspectral remote sensing of foliar
778 nitrogen content. *Proceedings of the National Academy of Sciences of the United States of America,*
779 *110*, E185-E192

780 Köhler, P., Guanter, L., Kobayashi, H., Walther, S., & Yang, W. (2018). Assessing the potential of
781 sun-induced fluorescence and the canopy scattering coefficient to track large-scale vegetation
782 dynamics in Amazon forests. *Remote Sensing of Environment, 204*, 769-785

783 Lewis, P., & Disney, M.I. (2007). Spectral invariants and scattering across multiple scales from
784 within-leaf to canopy. *Remote Sensing of Environment, 109*, 196-206

785 Li, W., Du, J., Li, S., Zhou, X., Duan, Z., Li, R., Wu, S., Wang, S., & Li, M. (2019). The variation
786 of vegetation productivity and its relationship to temperature and precipitation based on the
787 GLASS-LAI of different African ecosystems from 1982 to 2013. *International Journal of*
788 *Biometeorology, 63*, 847-860

789 Liu, H.Q., & Huete, A. (1995). A Feedback Based Modification of the NDVI to Minimize Canopy
790 Background and Atmospheric Noise. *Ieee Transactions on Geoscience and Remote Sensing, 33*,
791 457-465

792 Lyapustin, A., Wang, Y., Xiong, X., Meister, G., Platnick, S., Levy, R., Franz, B., Korkin, S., Hilker,
793 T., Tucker, J., Hall, F., Sellers, P., Wu, A., & Angal, A. (2014). Scientific impact of MODIS C5
794 calibration degradation and C6+ improvements. *Atmospheric Measurement Techniques, 7*, 4353-
795 4365

796 Marshak, A., & Knyazikhin, Y. (2017). The spectral invariant approximation within canopy
797 radiative transfer to support the use of the EPIC/DSCOVR oxygen B-band for monitoring
798 vegetation. *Journal of Quantitative Spectroscopy and Radiative Transfer, 191*, 7-12

799 Martínez-Vilalta, J., & Lloret, F. (2016). Drought-induced vegetation shifts in terrestrial
800 ecosystems: The key role of regeneration dynamics. *Global and Planetary Change, 144*, 94-108

801 Mercado, L.M., Bellouin, N., Sitch, S., Boucher, O., Huntingford, C., Wild, M., & Cox, P.M.
802 (2009). Impact of changes in diffuse radiation on the global land carbon sink. *Nature, 458*, 1014-
803 1017

804 Moparthy, S., Carrer, D., & Ceamanos, X. (2019). Can We Detect the Brownness or Greenness of
805 the Congo Rainforest Using Satellite-Derived Surface Albedo? A Study on the Role of Aerosol
806 Uncertainties. *Sustainability, 11*, 1410

807 Morton, D.C., Nagol, J., Carabajal, C.C., Rosette, J., Palace, M., Cook, B.D., Vermote, E.F.,
808 Harding, D.J., & North, P.R.J. (2014). Amazon forests maintain consistent canopy structure and
809 greenness during the dry season. *Nature, 506*, 221-224

810 Mu, Q., Heinsch, F.A., Zhao, M., & Running, S.W. (2007). Development of a global
811 evapotranspiration algorithm based on MODIS and global meteorology data. *Remote Sensing of*
812 *Environment, 111*, 519-536

Mu, Q., Zhao, M., & Running, S.W. (2011). Improvements to a MODIS global terrestrial evapotranspiration algorithm. *Remote Sensing of Environment, 115*, 1781-1800

Myneni, R.B., Yang, W., Nemani, R.R., Huete, A.R., Dickinson, R.E., Knyazikhin, Y., Didan, K., Fu, R., Negrón Juárez, R.I., Saatchi, S.S., Hashimoto, H., Ichii, K., Shabanov, N.V., Tan, B., Ratana, P., Privette, J.L., Morisette, J.T., Vermote, E.F., Roy, D.P., Wolfe, R.E., Friedl, M.A., Running, S.W., Votava, P., El-Saleous, N., Devadiga, S., Su, Y., & Salomonson, V.V. (2007). Large seasonal swings in leaf area of Amazon rainforests. *Proceedings of the National Academy of Sciences, 104*, 4820-4823

Ndehedehe, C.E., Ferreira, V.G., & Agutu, N.O. (2019). Hydrological controls on surface vegetation dynamics over West and Central Africa. *Ecological Indicators, 103*, 494-508

Nicholson, S.E. (2018). The ITCZ and the Seasonal Cycle over Equatorial Africa. *Bulletin of the American Meteorological Society, 99*, 337-348

Oliveira, R.S., Dawson, T.E., Burgess, S.S.O., & Nepstad, D.C. (2005). Hydraulic redistribution in three Amazonian trees. *Oecologia, 145*, 354-363

Philippon, N., Cornu, G., Monteil, L., Gond, V., Moron, V., Pergaud, J., Sèze, G., Bigot, S., Camberlin, P., Doumenge, C., Fayolle, A., & Ngomanda, A. (2019). The light-deficient climates of western Central African evergreen forests. *Environmental Research Letters, 14*, 034007

Piao, S., Wang, X., Park, T., Chen, C., Lian, X., He, Y., Bjerke, J.W., Chen, A., Ciais, P., Tømmervik, H., Nemani, R.R., & Myneni, R.B. (2020). Characteristics, drivers and feedbacks of global greening. *Nature Reviews Earth & Environment, 1*, 14-27

Pierret, A., Maeght, J.-L., Clément, C., Montoroi, J.-P., Hartmann, C., & Gonkhamdee, S. (2016). Understanding deep roots and their functions in ecosystems: an advocacy for more unconventional research. *Annals of Botany, 118*, 621-635

Pires, G.F., & Costa, M.H. (2013). Deforestation causes different subregional effects on the Amazon bioclimatic equilibrium. *Geophysical Research Letters, 40*, 3618-3623

Raghavendra, A., Zhou, L., Jiang, Y., & Hua, W. (2018). Increasing extent and intensity of thunderstorms observed over the Congo Basin from 1982 to 2016. *Atmospheric Research, 213*, 17-26

Raghavendra, A., Zhou, L., Roundy, P.E., Jiang, Y., Milrad, S.M., Hua, W., & Xia, G. (2020). The MJO's impact on rainfall trends over the Congo rainforest. *Climate Dynamics, 54*, 2683-2695

Rouse, J.W., Haas, R.H., Schell, J.A., & Deering, D.W. (1974). Monitoring Vegetation Systems in the Great Plains with Erts. In, *Third Earth Resources Technology Satellite-1 Symposium- Volume I: Technical Presentations*. Washington, D.C.: NASA

Rutan, D.A., Kato, S., Doelling, D.R., Rose, F.G., Nguyen, L.T., Caldwell, T.E., & Loeb, N.G. (2015). CERES Synoptic Product: Methodology and Validation of Surface Radiant Flux. *Journal of Atmospheric and Oceanic Technology, 32*, 1121-1143

Samanta, A., Knyazikhin, Y., Xu, L., Dickinson, R.E., Fu, R., Costa, M.H., Saatchi, S.S., Nemani, R.R., & Myneni, R.B. (2012). Seasonal changes in leaf area of Amazon forests from leaf flushing and abscission. *Journal of Geophysical Research: Biogeosciences, 117*

Song, W., Knyazikhin, Y., Wen, G., Marshak, A., Mõttus, M., Yan, K., Yang, B., Xu, B., Park, T., & Chen, C. (2018). Implications of Whole-Disc DSCOVR EPIC Spectral Observations for Estimating Earth's Spectral Reflectivity Based on Low-Earth-Orbiting and Geostationary Observations. *Remote Sensing, 10*, 1594

Sorí, R., Nieto, R., Vicente-Serrano, S.M., Drumond, A., & Gimeno, L. (2017). A Lagrangian perspective of the hydrological cycle in the Congo River basin. *Earth System Dynamic, 8*, 653-675

Wan, Z. (2014). New refinements and validation of the collection-6 MODIS land-surface temperature/emissivity product. *Remote Sensing of Environment, 140*, 36-45

Wang, D., Morton, D., Masek, J., Wu, A., Nagol, J., Xiong, X., Levy, R., Vermote, E., & Wolfe, R. (2012). Impact of sensor degradation on the MODIS NDVI time series. *Remote Sensing of Environment, 119*, 55-61

Wang, Y., Buermann, W., Stenberg, P., Smolander, H., H‰me, T., Tian, Y., Hu, J., Knyazikhin, Y., & Myneni, R.B. (2003). A new parameterization of canopy spectral response to incident solar radiation: case study with hyperspectral data from pine dominant forest. *Remote Sensing of Environment, 85*, 304-315

Xu, L., Saatchi, S.S., Yang, Y., Myneni, R.B., Frankenberg, C., Chowdhury, D., & Bi, J. (2015). Satellite observation of tropical forest seasonality: spatial patterns of carbon exchange in Amazonia. *Environmental Research Letters, 10*, 084005

Xu, L., Samanta, A., Costa, M.H., Ganguly, S., Nemani, R.R., & Myneni, R.B. (2011). Widespread decline in greenness of Amazonian vegetation due to the 2010 drought. *Geophysical Research Letters, 38*

Yan, D., Zhang, X., Yu, Y., & Guo, W. (2016a). A Comparison of Tropical Rainforest Phenology Retrieved From Geostationary (SEVIRI) and Polar-Orbiting (MODIS) Sensors Across the Congo Basin. *IEEE Transactions on Geoscience and Remote Sensing, 54*, 4867-4881

Yan, D., Zhang, X., Yu, Y., & Guo, W. (2017). Characterizing Land Cover Impacts on the Responses of Land Surface Phenology to the Rainy Season in the Congo Basin. *Remote Sensing, 9*, 461

Yan, K., Park, T., Yan, G., Chen, C., Yang, B., Liu, Z., Nemani, R.R., Knyazikhin, Y., & Myneni, R.B. (2016b). Evaluation of MODIS LAI/FPAR Product Collection 6. Part 1: Consistency and Improvements. *Remote Sensing, 8*, 359

Yan, K., Park, T., Yan, G., Liu, Z., Yang, B., Chen, C., Nemani, R.R., Knyazikhin, Y., & Myneni, R.B. (2016c). Evaluation of MODIS LAI/FPAR Product Collection 6. Part 2: Validation and Intercomparison. *Remote Sensing, 8*, 460

886 Yang, B., Knyazikhin, Y., Mottus, M., Rautiainen, M., Stenberg, P., Yan, L., Chen, C., Yan, K.,
887 Choi, S., Park, T., & Myneni, R.B. (2017). Estimation of leaf area index and its sunlit portion from
888 DSCOVR EPIC data: Theoretical basis. *Remote Sensing of Environment, 198*, 69-84

889 Yang, J., Tian, H., Pan, S., Chen, G., Zhang, B., & Dangal, S. (2018a). Amazon drought and forest
890 response: Largely reduced forest photosynthesis but slightly increased canopy greenness during
891 the extreme drought of 2015/2016. *Global Change Biology, 24*, 1919-1934

892 Yang, Y., Saatchi, S.S., Xu, L., Yu, Y., Choi, S., Phillips, N., Kennedy, R., Keller, M., Knyazikhin,
893 Y., & Myneni, R.B. (2018b). Post-drought decline of the Amazon carbon sink. *Nature*
894 *Communications, 9*, 3172

895 Zhang, Y., Song, C., Band, L.E., Sun, G., & Li, J. (2017). Reanalysis of global terrestrial vegetation
896 trends from MODIS products: Browning or greening? *Remote Sensing of Environment, 191*, 145-
897 155

898 Zhou, L., Tian, Y., Myneni, R.B., Ciais, P., Saatchi, S., Liu, Y.Y., Piao, S., Chen, H., Vermote, E.F.,
899 Song, C., & Hwang, T. (2014). Widespread decline of Congo rainforest greenness in the past
900 decade. *Nature, 509*, 86-90

901

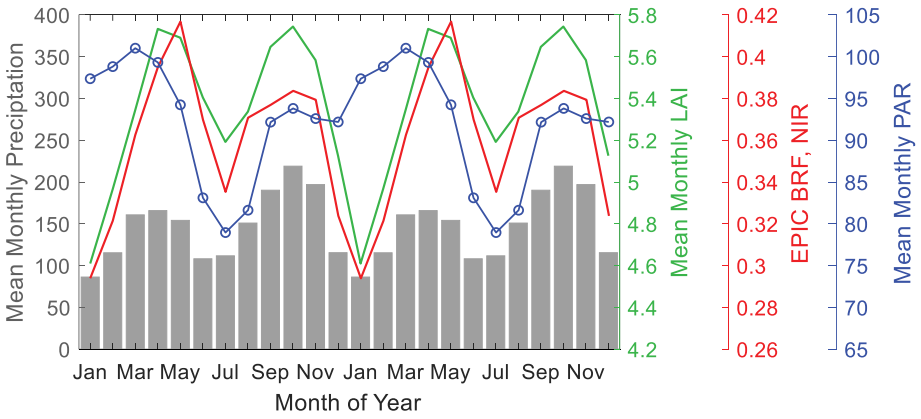

Fig. 1. Annual course of monthly-average precipitation, PAR, LAI, EPIC NIR BRF over the Congolese forests. The annual cycle is repeated two times for better demonstration. Precipitation, LAI and NIR BRF clear show bimodal variations with peaks in March-April-May (MAM, wet season 1) and September-October-November (SON, wet season 2).

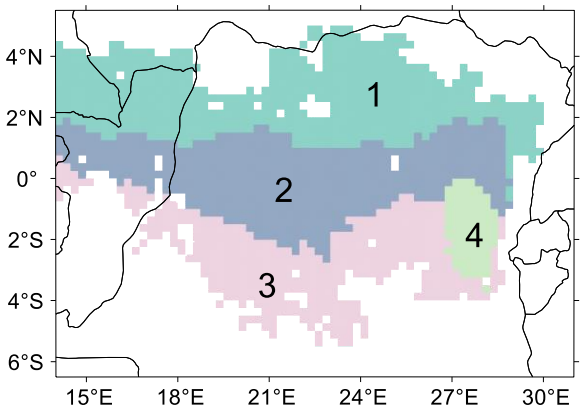

Fig. 2. Four phenological regions clustered based on normalized 20-year mean monthly climatology of precipitation, PAR and LAI data using K-Means clustering method. Region 4 (0.2°S-3°S, 26.8°E-28.5°E) represents montane forests located at moderate elevations between 530 m and 1728 m.

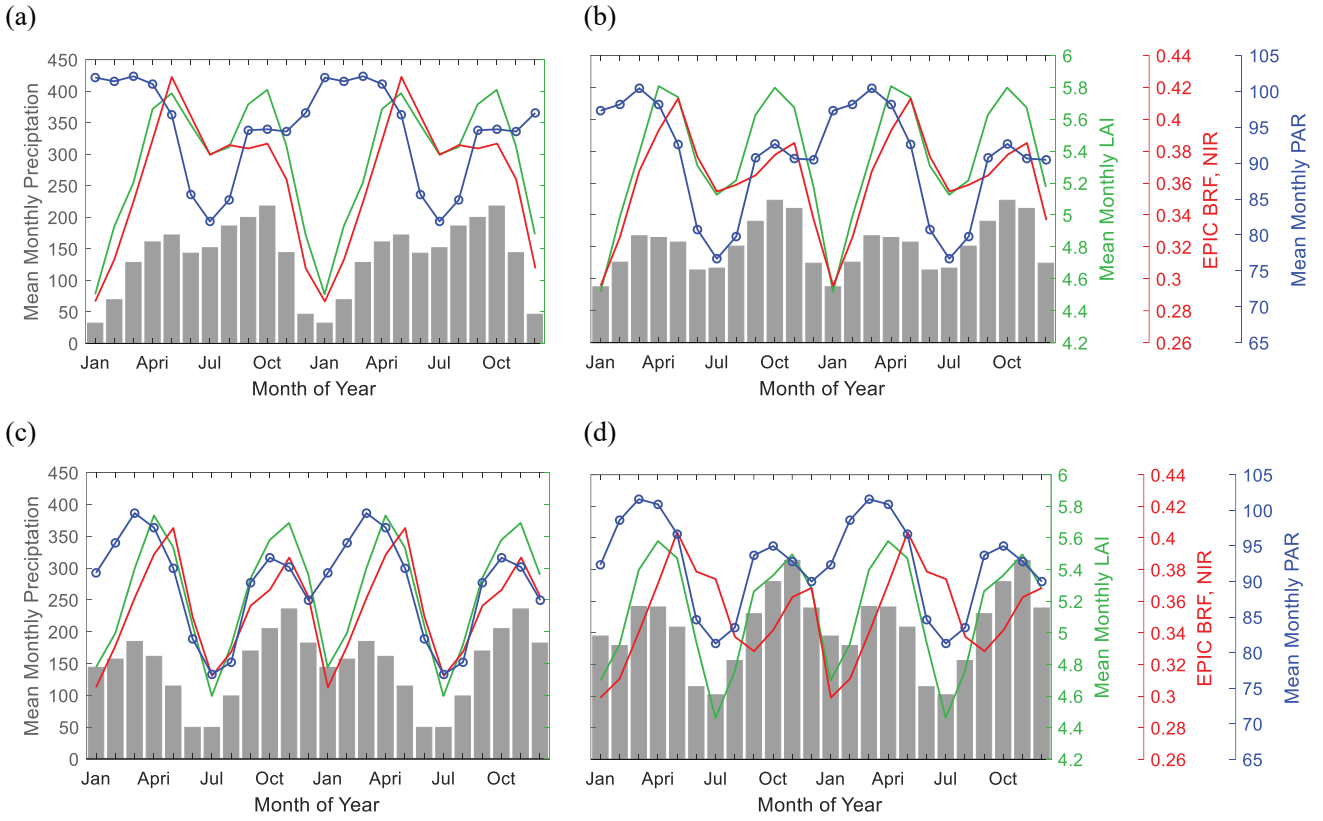

Fig. 3. Annual course of monthly-average precipitation, PAR, LAI, EPIC NIR BRF over (a) region 1, (b) region 2, (c) region 3 and (d) region 4. Phenological regions are shown in Figure 2. The annual cycles are replicated two times for better demonstration. The peak-to-peak amplitude of bimodal curves tends to increase from north (region 1) to south (region 3).

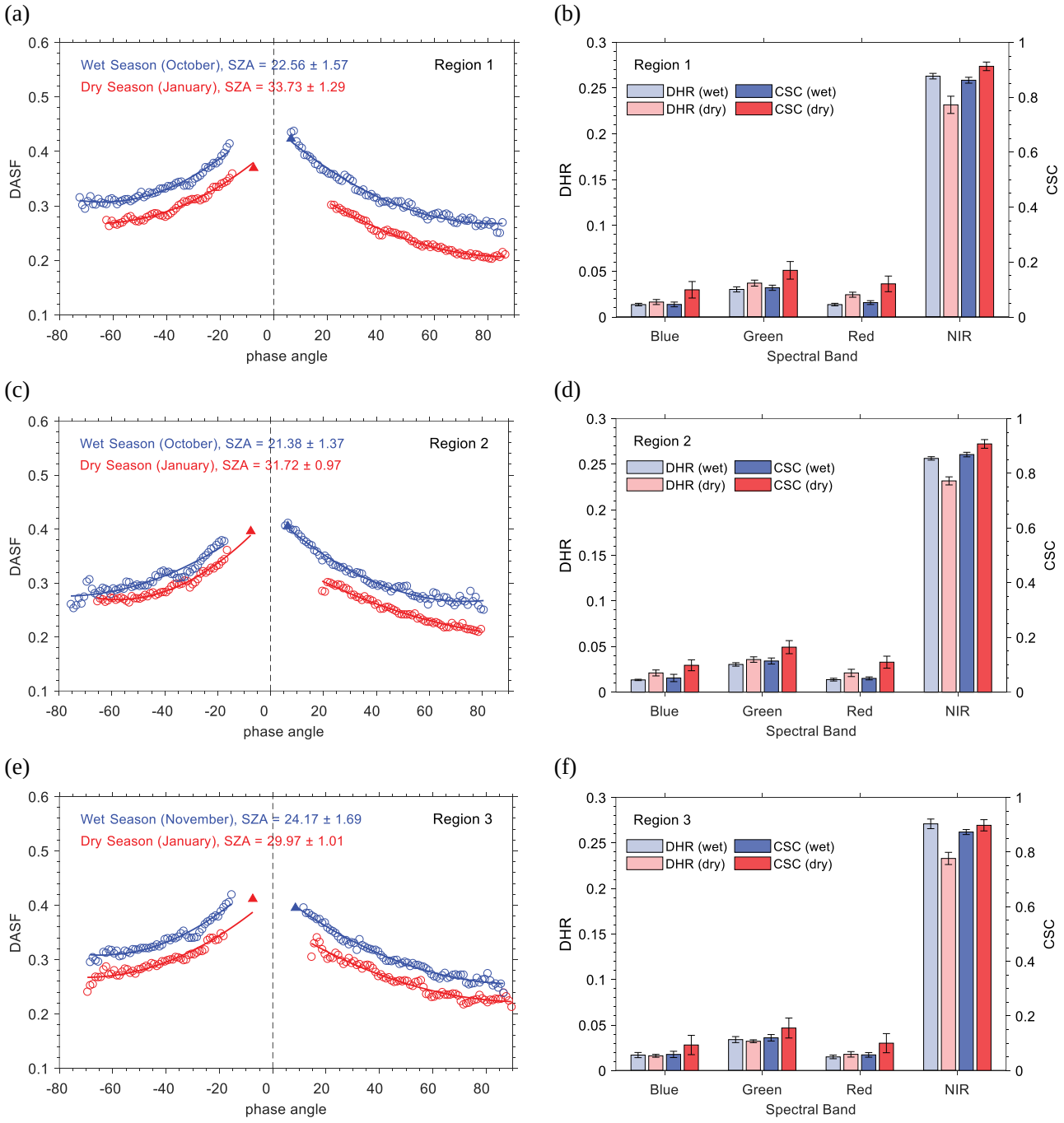

Fig. 4. Directional Area Scattering Factors (DASF) derived from MISR and DSCOVR EPIC data (left panels), MISR Directional Hemispherical Reflectances (DHR) and Canopy Scattering Coefficients (CSC) during wet and dry seasons over region 1 (panels a and b), region 2 (panels c and d) and region 3 (panels e and f). The circles and solid triangles represent MISR and DSCOVR EPIC observations. The lines show polynomial fits to MISR data. There were no enough valid reflectance data over region 3 in October. Therefore, we use November to represent the dry season in this region.

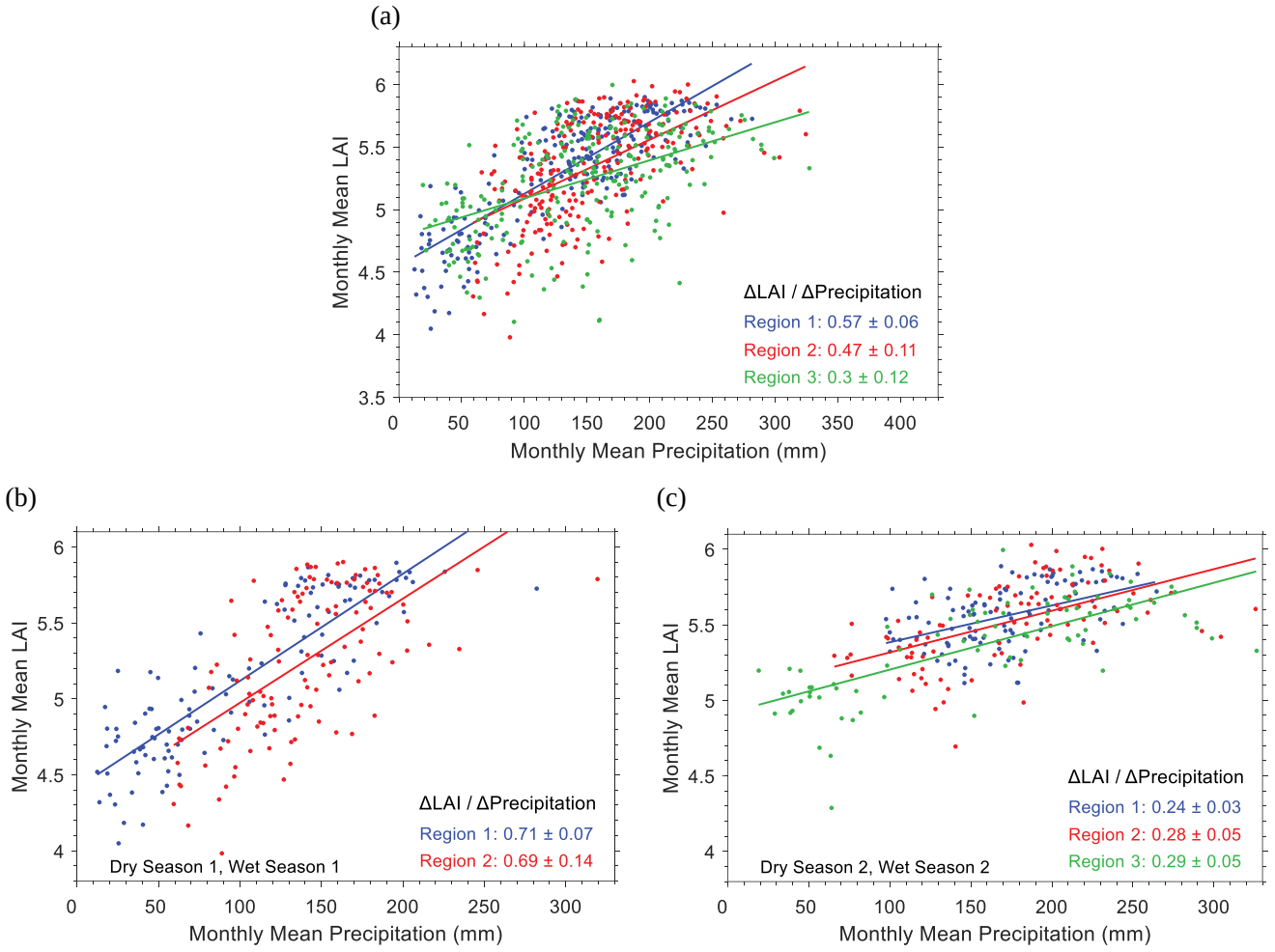

Fig. 5. Relationship between regional monthly precipitation and LAI during (a) full annual seasonal cycle, (b) seasonal cycle 1 (December-May) and (c) cycle 2 (June-November). Slopes of the regression lines are taken as a measure of LAI sensitivity to changes in in the precipitation (ΔLAI/ΔPrecipitation).

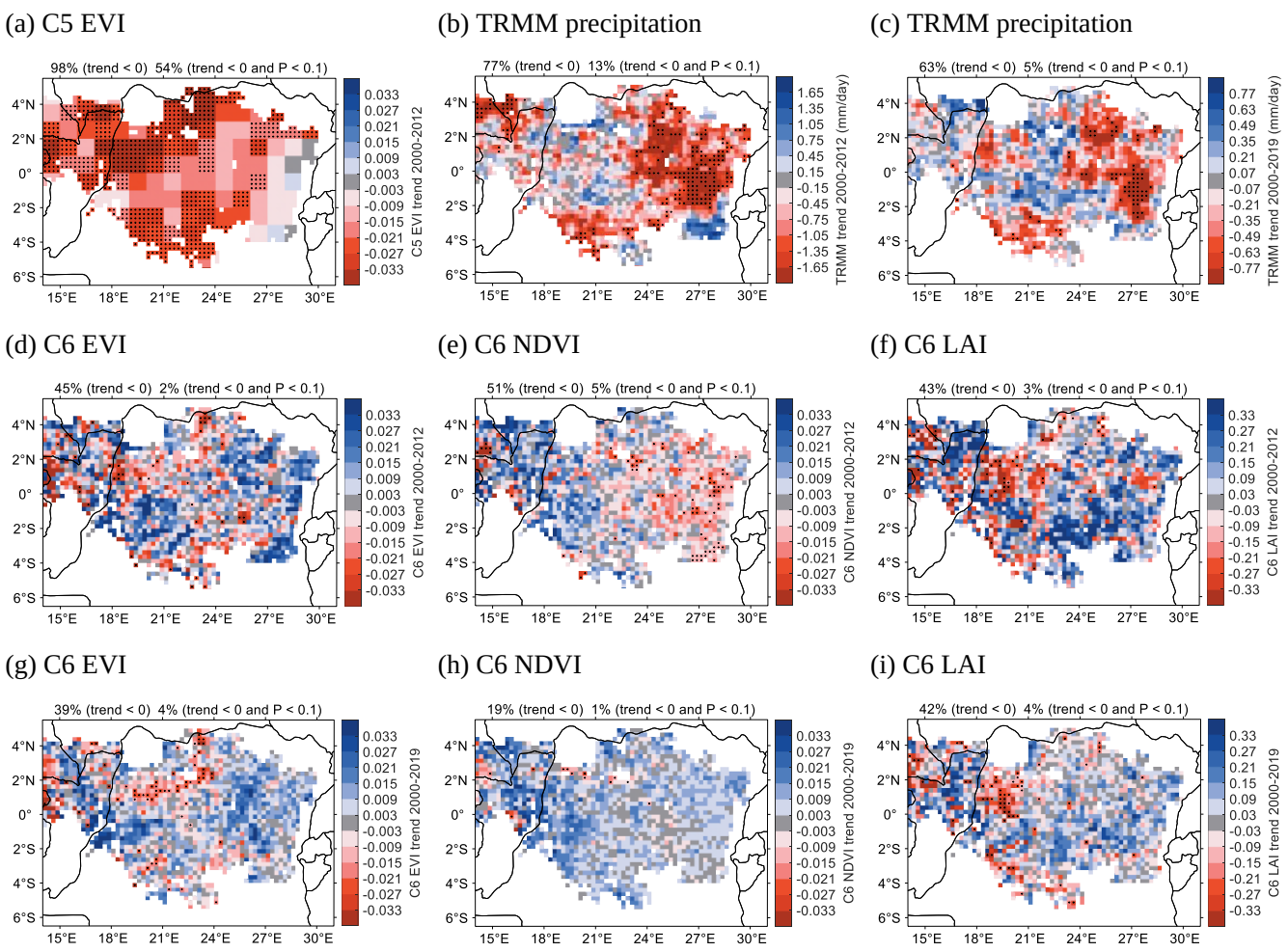

Fig. 6. Linear trends per decade in April-May-June for the period of 2000-2012 and 2000-2019. Pixels with the plus symbol indicate statistically significant trends (P<0.1). Percentages of pixels with negative trends and negative trends at P<0.1 are shown above each plot. The upper plots show trends in MODIS Collection 5 EVI from 2000 to 2012 (panel a) and TRMM precipitations for the 2000 to 2012 (panel b) and 2000 to 2019 (panel c) periods. Trends in MOIDIS Collection 6 EVI, NDVI and LAI for the 2000 to 2012 and the 2000 to 2019 periods are shown in middle and lower plots, respectively.

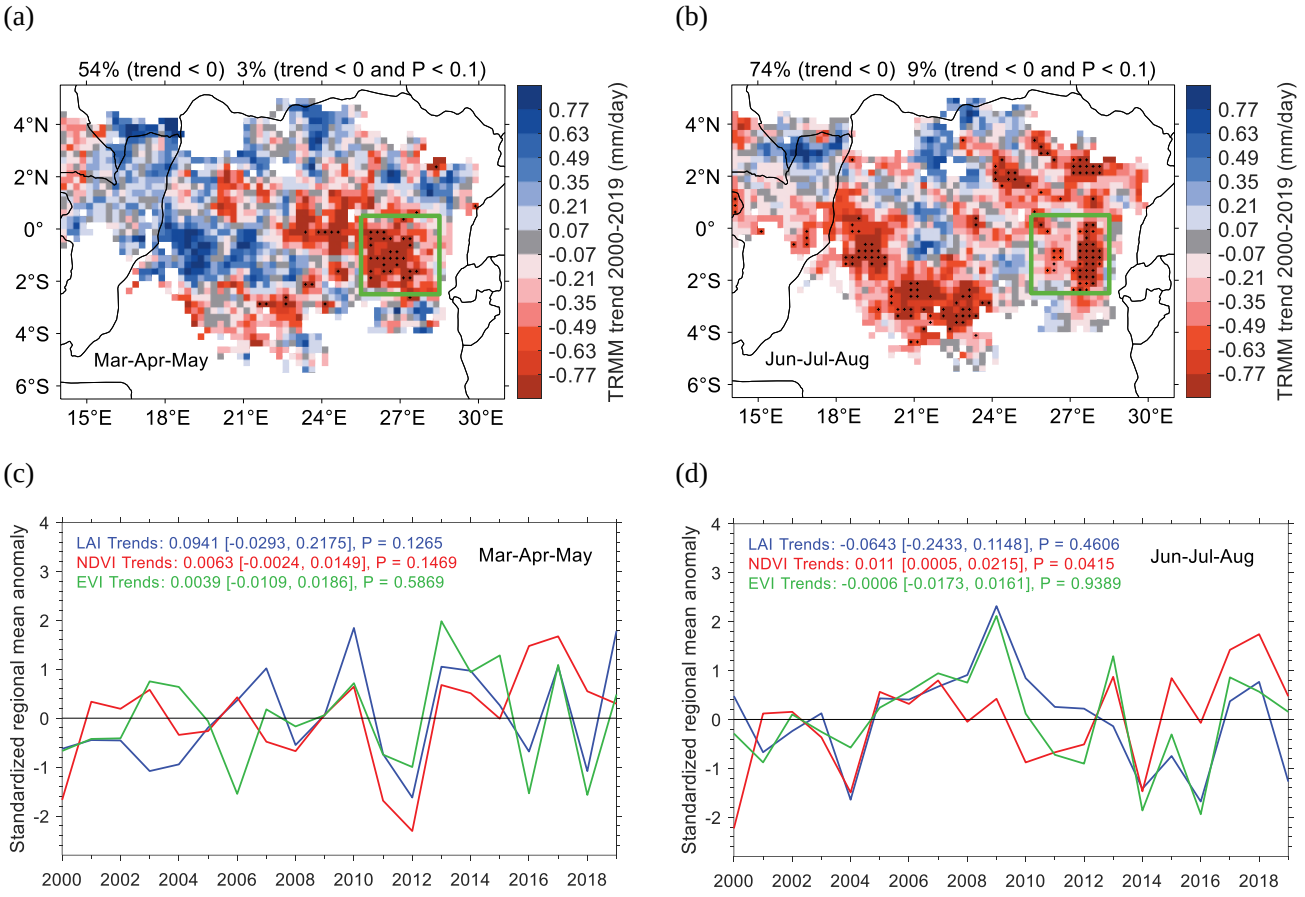

Fig. 7. Upper panels. Precipitation linear trends per decade during (a) wet season 1 (MAM) and (b) dry season 2 (JJA) for the period of 2000-2019. Pixels with the plus symbols indicate statistically significant trends (P<0.1). A region between 0.5°N-2.5°S and 25.5°E-28.5°E where a significant precipitation decline was observed both during the wet and dry seasons is shown as a green rectangle. Lower panels. Standardized regional mean anomalies in LAI, NDVI and EVI for the selected region during (c) wet (MAM) and (d) dry (JJA) seasons for the 2000-2019 period. The linear trend (with 95% confidence interval) per decade and its significance level P are shown in legends.

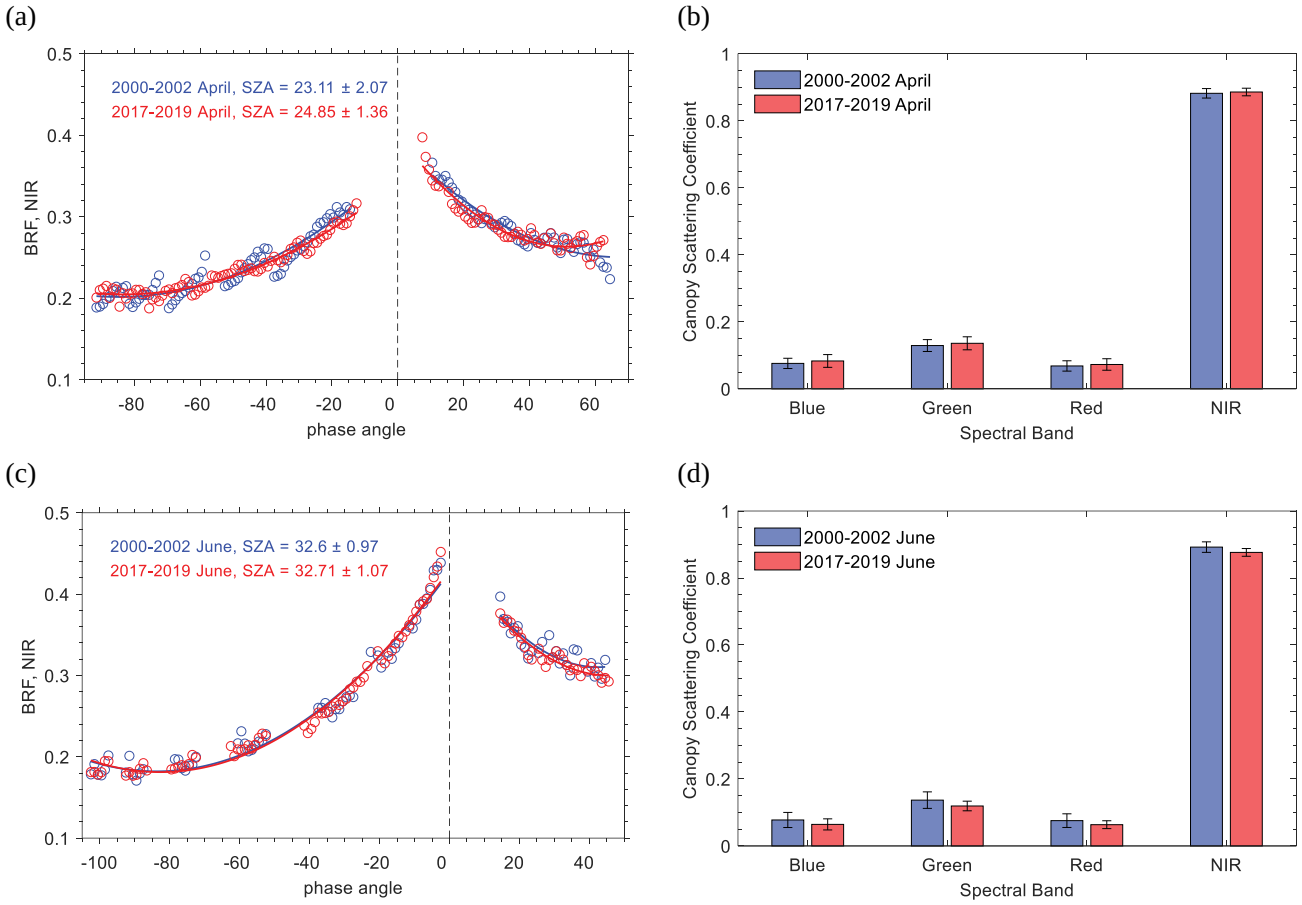

Fig. 8. MISR BRF at NIR (866 nm) and canopy scattering coefficient (right panels) of the region with significant drought at the beginning (2000-2002) and at the end (2017-2019) of the 2000-2019 observation period. Upper and lower panels show BRF and the coefficient in April (wet season) and June (dry season), respectively. These variables other months show similar behavior.

Table 1

Brief information of variables and datasets used in this study.

Variable	Product	Spatial resolution	Temporal resolution
LAI	C6 MOD15A2H & MYD15A2H	500 m	8 day
EVI	C6 MOD13C2	0.05°	monthly
EVI	C5 MODVI	1°	monthly
NDVI	C6 MOD13C2	0.05°	monthly
Land cover	C6 MCD12C1	0.05°	yearly
LST	C6 MYD11C3	0.05°	monthly
Evapotranspiration	C6 MOD16A2	500 m	8 day
Precipitation	TRMM	0.25°	monthly
PAR	CERES	1°	monthly
BRF	Terra MISR	1.1 km	16 day
DHR	Terra MISR	1.1 km	16 day
BRF	DSCOVR EPIC	10 km	65 to 110 min

Table 2

Pearson's correlation coefficients of regional mean monthly LAI and precipitation and PAR over different region and different seasonal cycle. (*P<0.1, **P<0.01)

		Cycle 1	Cycle 2	annual
R (TRMM, LAI)	Entire region	0.68**	0.59**	0.63**
	Region 1	0.81**	0.41**	0.78**
	Region 2	0.58*	0.55**	0.56**
	Region 3	0.13	0.65**	0.48**
R (PAR, LAI)	Entire region	0.01	0.67**	-0.01
	Region 1	-0.17*	0.46**	-0.29**
	Region 2	-0.07	0.64**	0.07
	Region 3	0.25**	0.73**	0.52**